

Supporting Information

Electrocatalytic water oxidation by copper(II) complexes containing a tetra- or pentadentate amine-pyridine ligand

Junyu Shen,^a Mei Wang,^{*a} Peili Zhang,^a Jian Jiang^a and Licheng Sun^{ab}

^a*State Key Laboratory of Fine Chemicals, DUT-KTH Joint Education and Research Center on Molecular Devices, Dalian University of Technology (DUT), Dalian 116024, China*

^b*Department of Chemistry, KTH Royal Institute of Technology, Stockholm 10044, Sweden*

Materials and instruments

Materials. Manipulations for preparation of the copper complexes were carried out under pure N₂ by using standard Schlenk techniques. Commercially available chemicals, Cu(BF₄)₂·6H₂O, benzaldehyde, 1,2-ethanediamine, and 2-(chloromethyl)pyridine hydrochloride, were purchased from local suppliers. Ampliflu red (AR) and horseradish peroxidase (HRP) were purchased from Aladdin. All reagents were used as received. Glassy carbon electrode, fluorine-doped tin oxide (FTO) glass plate, and platinum foil were purchased from Tianjin Gauss Union for the electrochemical studies. All buffers were prepared with deionized water (18 MΩ·cm resistivity).

Instruments. NMR Spectra were collected with a Varian INOVA 400 NMR spectrometer. Mass spectra were recorded with HP 1100 HPL/ESI-DAD-MS and Waters/Micromass LC/Q-TOF-MS instruments. Elemental analyses were performed with a Thermoquest-Flash EA 1112 elemental analyzer. UV-Vis absorption measurements were carried out on an Agilent 8453 spectrophotometer. SEM images and EDX spectra were obtained with a FEI Nova NanoSEM 450 instrument equipped with an EDX detector. XPS surveys were acquired with a ThermoFisher ESCALAB 250Xi surface analysis system. The ICP-OES results were

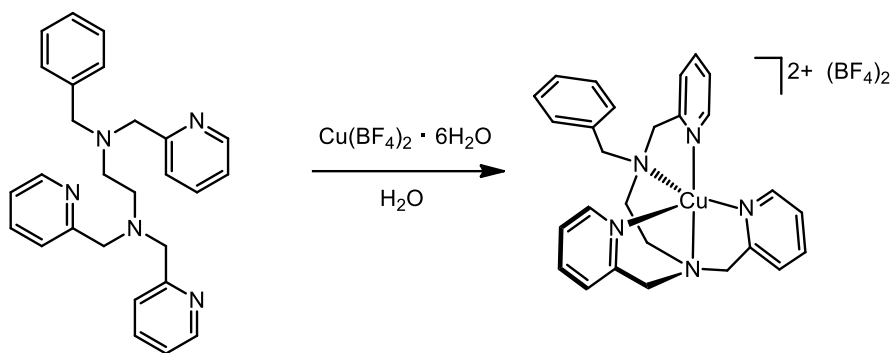
obtained with a Perkin Elmer 2000 DV ICP optical emission spectrometer. After 5 h of electrolysis, we found that a slight amount of copper was deposited on the surface of the Pt plate cathode. The used Pt plate was immersed in aqua regia to dissolve the deposited material, and the resulting solution was analyzed by the inductively coupled plasma optical emission spectroscopy (ICP-OES) to determine the amount of completely reduced copper complex. Dynamic light scattering (DLS) spectra were measured with a Zetasizer Nano ZS90 instrument.

Synthesis

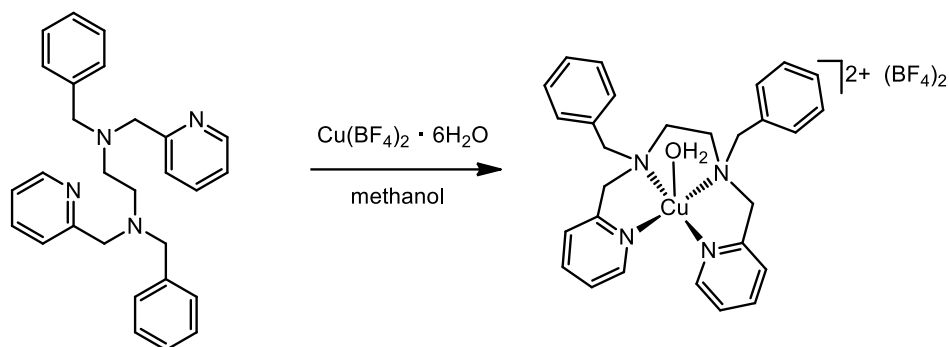
Preparation of bztpen ligand. Diamine-tripyridine ligand, *N*-benzyl-*N,N',N'*-tris(pyridin-2-ylmethyl)ethylenediamine (bztpen), was prepared according to the literature procedure.^{S1,S2} Anal. Calcd for C₂₇H₂₉N₅ (%): C 76.56, H 6.90, N 16.53; found: C 76.65, H 6.83, N 16.60. ¹H NMR (CDCl₃, 400 MHz): δ 8.48 (3H, m), 7.58 (3H, t, *J* = 6.4 Hz), 7.47 (3H, t, *J* = 6.3 Hz), 7.18–7.30 (5H, m), 7.12 (3H, m), 3.77 (4H, s), 3.72 (2H, s), 3.59 (2H, s) and 2.73 (4H, m). ¹³C NMR (CDCl₃, 400 MHz): δ 160.16, 159.73, 148.94, 148.79, 139.18, 136.30, 128.71, 128.17, 126.88, 122.71, 122.65, 121.84, 121.78, 60.78, 60.59, 58.91, 52.20 and 51.89. ESI-MS: Calcd for [M+H]⁺: *m/z* = 424.24; found: *m/z* = 424.21.

Preparation of dbzbpen ligand. Diamine-dipyridine ligands, *N,N'*-dibenzyl-*N,N'*-bis(pyridin-2-ylmethyl)ethylenediamine (dbzbpen), was prepared according to the literature procedure.^{S3} Anal. Calcd for C₂₈H₃₀N₄ (%): C 79.59, H 7.16, N 13.26; found: C 79.62, H 6.96, N 13.45. ¹H NMR (CDCl₃, 400 MHz): δ 8.48 (d, 2H, *J* = 5.0 Hz), 7.57 (m, 2H), 7.45 (d, 2H, *J* = 8.1 Hz), 7.25–7.32 (m, 10H), 7.11 (m, 2H), 3.70 (s, 4H), 3.57 (s, 4H), 2.68 (s, 4H). ¹³C NMR (CDCl₃, 400 MHz): δ 159.22, 147.75, 138.31, 135.21, 127.71, 127.13, 125.82, 121.64, 120.70, 59.57, 57.95 and 50.77. ESI-MS: Calcd for [M+H]⁺: *m/z* = 423.25; found: *m/z* = 423.24.

Preparation of [(bztpen)Cu](BF₄)₂ (1).^{S4} Compound Cu(BF₄)₂ · 6H₂O (0.345 g, 1.0 mmol) was added into an aqueous solution (40 mL) of bztpen (0.423 g, 1.0 mmol) with magnetic stirring. The mixture was stirred under nitrogen at room temperature for 8 h. The blue solution was then concentrated to about 10 mL by evaporation under vacuum and stood at room temperature for 2 days. Light blue crystals were obtained in a yield of 85% (0.55 g). Anal. Calcd for C₂₇H₂₉N₅B₂F₈Cu · H₂O (%): C 47.78, H 4.60, N 10.32; found: C 47.86, H 4.66, N 10.36. TOF-MS: Calcd for [M - 2BF₄]²⁺ (C₂₇H₂₉N₅Cu): *m/z* = 243.0854; found: *m/z* = 243.0852.



Preparation of [(dzbpen)Cu(OH₂)](BF₄)₂ (2): Compound Cu(BF₄)₂ · 6H₂O (0.345 g, 1.0 mmol) was added to a methanol solution (40 mL) of dzbpen (0.422 g, 1.0 mmol). The mixture was stirred under N₂ at room temperature for 8 h. The blue solution was then concentrated to about 20 mL by evaporation under vacuum. Light blue crystals were formed with diffusion of diethyl ether into the resulting solution and obtained in a yield of 86% (0.58 g). Anal. Calcd for C₂₈H₃₂N₄O₂F₈Cu (%): C 49.62, H 4.76, N 8.27; found: C 48.73, H 4.71, N 8.27. TOF-MS: Calcd for [M - H₂O - 2BF₄]²⁺ (C₂₈H₃₀N₄Cu): *m/z* = 242.5860; found: *m/z* = 242.5872.



Crystallographic structure determinations

The single-crystal X-ray diffraction data were collected on a Bruker Smart Apex II CCD diffractometer with a graphite-monochromated Mo- K_α radiation ($\lambda = 0.071073 \text{ \AA}$) at 296 K using the ω - 2θ scan mode. Data processing was accomplished with the SAINT processing program.^{S5} Intensity data were corrected for absorption by the SADABS program.^{S6} All structures were solved by direct methods and refined on F^2 against full-matrix least-squares methods by using the SHELXTL 97 program package.^{S7} Non-hydrogen atoms were refined anisotropically. Hydrogen atoms were located by geometrical calculation. Crystallographic data and selected bond lengths and angles for **1** and **2** are given in Tables S1 and S2 (CCDC-1058390 for **1** and -1526265 for **2**).

Electrochemistry studies

All electrochemical measurements were performed with a model CHI660E electrochemical workstation (CH instruments).

CV measurements. Cyclic voltammetry experiments were carried out in a three-electrode cell under argon. The working electrode was a glassy carbon electrode disc (0.071 cm^2) polished with 3 and 1 μm diamond pastes and sonicated in ion-free water for 15 min prior to use. The reference electrode was an aqueous Ag/AgCl electrode and the counter electrode was a platinum wire. The solution of 0.1 M phosphate buffer was used as supporting electrolyte,

which was degassed by bubbling with argon for 15 min before measurement. Potentials were measured using a Ag/AgCl reference electrode and are reported versus the normal hydrogen electrode (NHE) by addition of 0.197 V to the experimentally measured values.

Controlled potential electrolysis (CPE) experiments. All CPE experiments made in water were carried out in a single cell except for measurements of Faradaic efficiency. A fluorine-doped tin oxide (FTO) with a surface area of 0.7 cm² was used as the working electrode for electrolysis conducted in aqueous media. The auxiliary electrode was a platinum plate (2 cm²) and the reference electrode was a commercially available aqueous Ag/AgCl electrode. The sample was bubbled with argon for 20 min before measurement and the CPE experiments were carried out under argon with constantly stirring.

Kinetics. Figs S12 and S13 recorded with varied concentrations of **1** and **2** from 0.33 to 1.33 mM in 0.1 M PBS at pH 11.5 show that the catalytic peak currents for water oxidation varies linearly with the concentration of catalyst, consistent with single-site molecular catalysis for water oxidation as observed for other reported N4 and N5 coordinated Cu^{II} electrocatalysts. In this case, the limiting catalytic current (i_c) can be estimated by eq. 1.^{S8}

$$i_c = n_c F A [\text{Cu}] (k_{\text{cat}} D_{\text{Cu}})^{1/2} \quad (\text{eq. 1})$$

where i_c is the limiting catalytic peak current, n_c is the number of electrons transferred for producing a molecule of O₂ in water oxidation ($n_c = 4$), F is Faraday constant, A is the surface area of the electrode (in cm²), $[\text{Cu}]$ is the initial concentration of catalyst (in mol L⁻¹), k_{cat} is the apparent first-order rate constant, and D_{Cu} is the diffusion coefficient of the copper catalyst in 0.1 M phosphate buffer at pH 11.5.

In the other aspect, the peak currents of **1** and **2**, both for the catalytic peak and for the noncatalytic wave of the Cu^{II}/Cu^I couple, vary linearly with the square root of the scan rate (Figs S14 and S15). This result is consistent with the Randles–Sevcik equation,

$$i_d = 0.4463 n_d F A [\text{Cu}] (n_d F v D_{\text{Cu}} / RT)^{1/2} \quad (\text{eq. 2})$$

where i_d is the plateau current density of noncatalytic wave (here taken from the reversible reduction wave of $\text{Cu}^{\text{I}}/\text{Cu}^{\text{II}}$ couple), n_d is the number of electron transferred for the $\text{Cu}^{\text{II}}/\text{Cu}^{\text{I}}$ couple ($n_d = 1$), v is the scan rate, R is the universal gas constant, and T is the temperature in Kelvin.

The ratio of eqs 1 and 2 gives eq 3,

$$i_c/i_d = 1.436(k_{\text{cat}}/v)^{1/2} \quad (\text{eq. 3})$$

From the slope of the plot of the ratio, i_c/i_d versus $v^{-1/2}$ in Fig. S16, $k_{\text{cat}1} = 13.1 \text{ s}^{-1}$ for **1** and $k_{\text{cat}2} = 18.7 \text{ s}^{-1}$ for **2** in 0.1 M phosphate buffer at pH 11.5 at 25 °C. For water oxidation, with water as both substrate and solvent, the measured value of k_{cat} is also the catalytic turnover frequency for catalytic water oxidation.

Determination of Faradaic efficiency. The CPE experiments of the solutions of **1** and **2** (both in 1 mM) were carried out in 0.1 M phosphate buffer (20 mL) at pH 11.5 in a custom built gas-tight electrochemical cell at an applied potential of 1.4 V vs NHE for 60 min with a FTO (surface area 0.7 cm²) working electrode. The gas in the headspace of the cell was analyzed by CEAULIGHT GC-7920 gas chromatograph equipped with a 5 Å molecular sieve column (2 mm × 2 m) during the electrolysis. The amount of oxygen generated was determined by GC with the external standard method and the background O₂ from cell leakage was deducted from the total amount of O₂. According to the O₂ volume evolved and the amount of O₂ calculated from the total consumed charge during the CPE experiment assuming a 4e⁻ catalytic process, the Faradaic efficiencies for electrochemical O₂ evolution are about 91(±1)% for **1** and 94(±2)% for **2** (Fig. S18).

Testing peroxide intermediates formed during CPE experiments in electrolytes.^{9,10} Ampliflu red (AR) was dissolved in DMSO and horseradish peroxidase (HRP) in 0.5 M PBS, both in a concentration of 0.4 mg mL⁻¹. Controlled potential electrolysis (CPE) experiments of **1** or **2** (3 mM) in pH 11.5 PBS were carried out at 1.4 V vs. NHE in an electrochemical cell

with cathode and anode isolated by a porous ceramic frit. A fluorine-doped tin oxide (FTO) with a surface area of 1.5 cm² was used as working electrode. After 2 h of electrolysis, the HRP solution (1.0 mL) and AR solution (1.0 mL) were successively added into the resulting electrolyte (0.3 mL). The blue color of the solution turned pink after the sample was shaken for about 1 minute (Fig. S28).

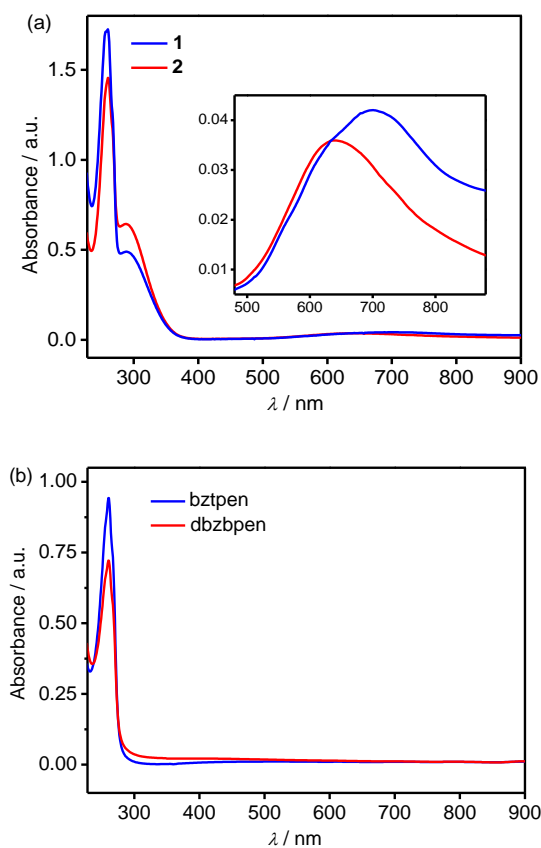


Fig. S1 (a) UV-vis spectra of **1** and **2** (both in 0.1 mM) in water. Inset: magnified views of weak absorptions of **1** and **2** in the region of 500–900 nm. Complexes **1** and **2** each display two intense ligand $\pi \rightarrow \pi^*$ absorptions at $\lambda_{\max} = 258\text{--}260$ and $289\text{--}290$ nm, together with a broad weak absorption arising from Cu^{II} d–d transitions, at $\lambda_{\max} = 700$ nm for **1** and 650 nm for **2**. (b) UV-vis spectra of ligands, bztpen and dbzpen (both in 0.1 mM), in 0.1 M PBS containing 10% methanol due to poor solubility of bztpen and dbzpen in water.

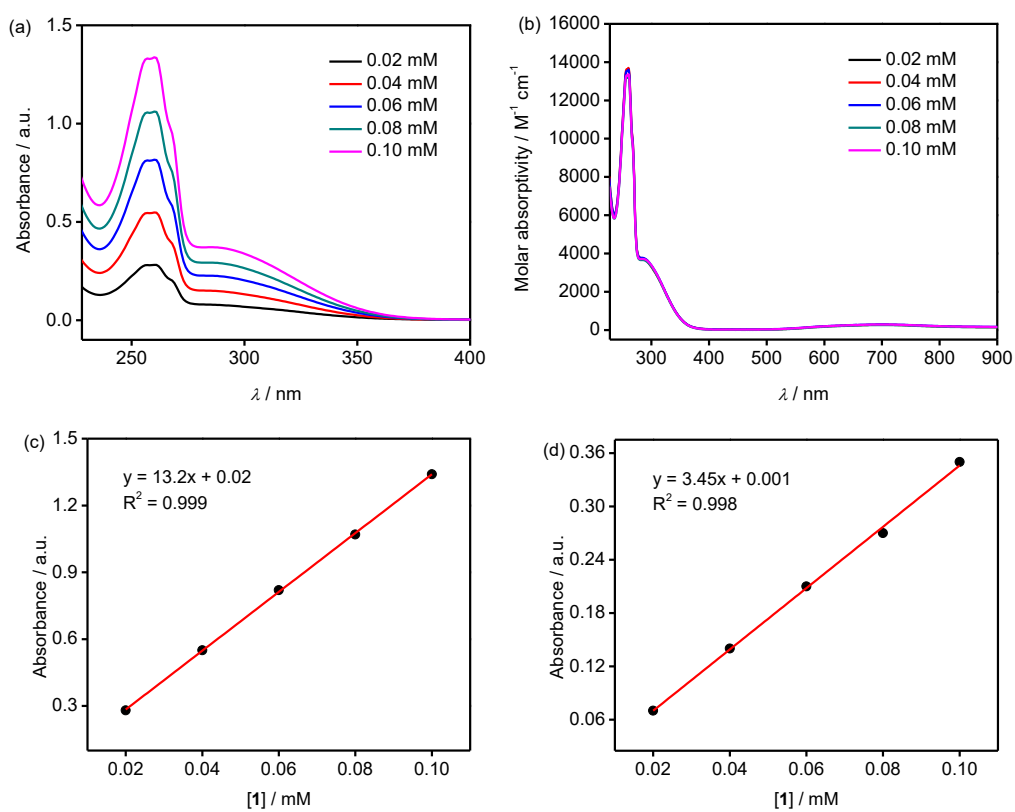


Fig. S2 (a), (b) UV-vis spectra of **1** in 0.1 M PBSs at pH 11.5 with the concentration varied from 0.02 to 0.10 mM. Plots of the absorbance intensity at 259 nm (c) and 298 nm (d) versus the concentration of **1**.

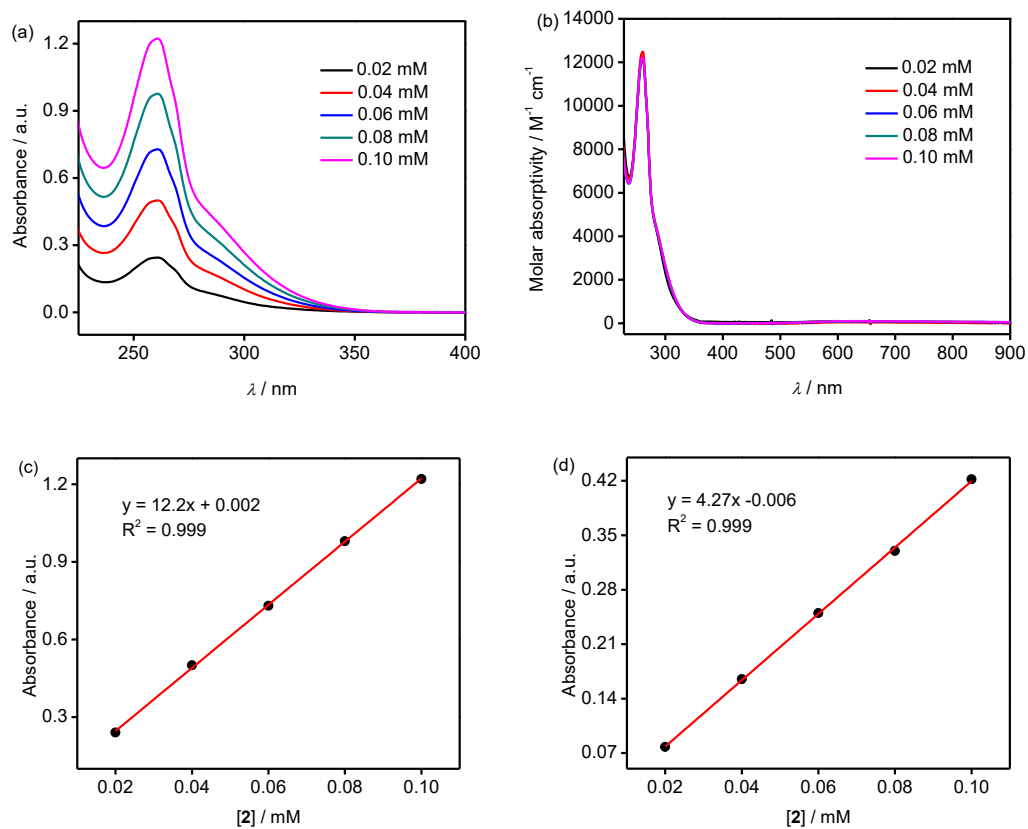


Fig. S3 (a), (b) UV-vis spectra of **2** in 0.1 M PBSs at pH 11.5 with the concentration varied from 0.02 to 0.10 mM. Plots of the absorbance intensity at 260 nm (c) and 287 nm (d) versus the concentration of **2**.

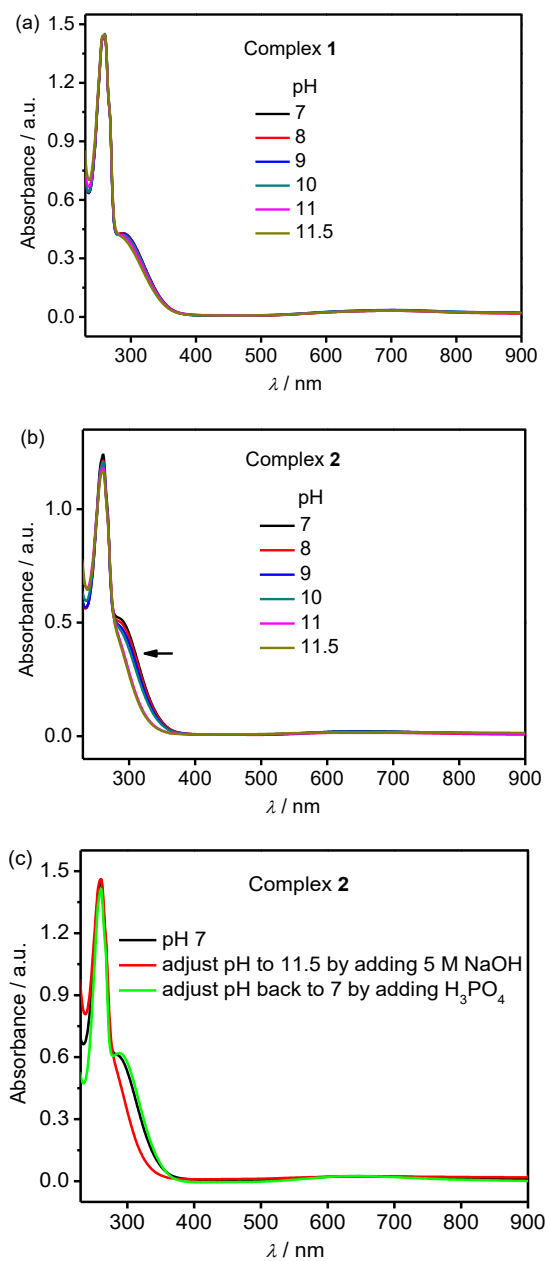


Fig. S4 UV-vis spectra of (a) **1** and (b) **2** in 0.1 M PBSs at varying pH values from 7 to 11.5.

(c) Adding phosphoric acid (85%) to the pH 11.5 solution of **2** to adjust the pH back to 7.

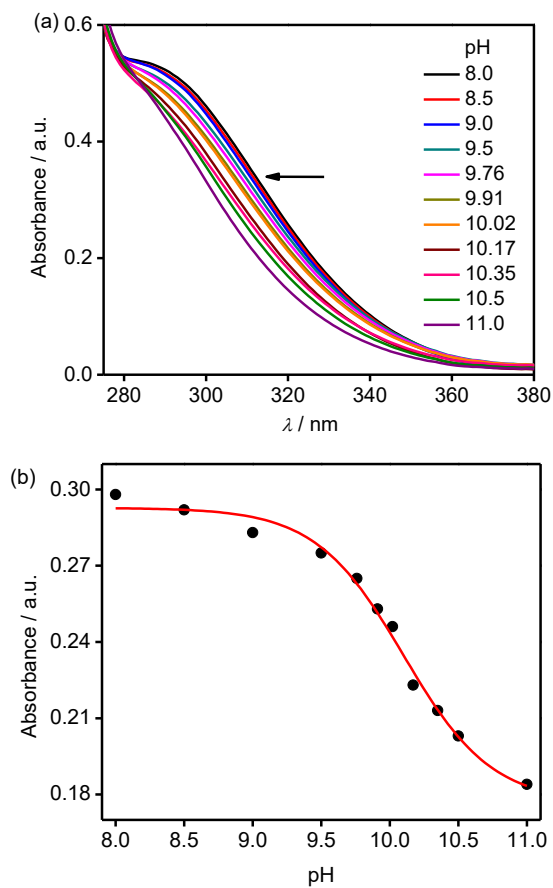


Fig. S5 (a) UV-vis spectra of **2** in 0.1 M PBSs at varying pH values from 8.0 to 11.0 at 25 °C. (b) Plot of the absorbance of **2** at $\lambda = 316$ nm as a function of pH in the range of 8.0–11.0. This plot shows the inflection point at pH = 10.1, which is the estimated pK_a value for **2**.

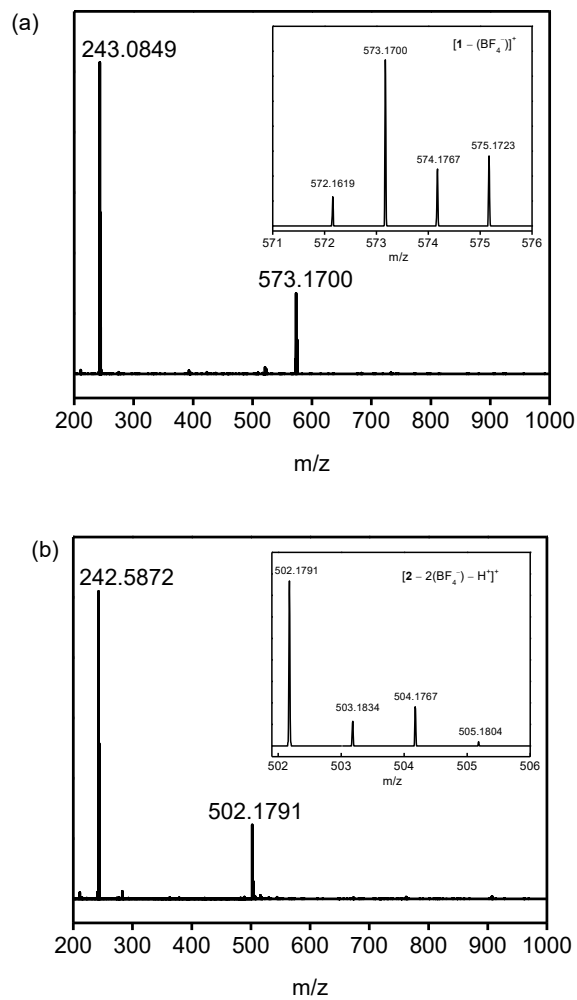


Fig. S6 The high-resolution mass spectra (ESI, 3.5 kV) of (a) **1** and (b) **2** in pH 11.5 aqueous solutions. Insets: high-resolution mass spectra of $[1-(\text{BF}_4^-)]^+$ and $[2-2(\text{BF}_4^-)-\text{H}^+]^+$ peaks.

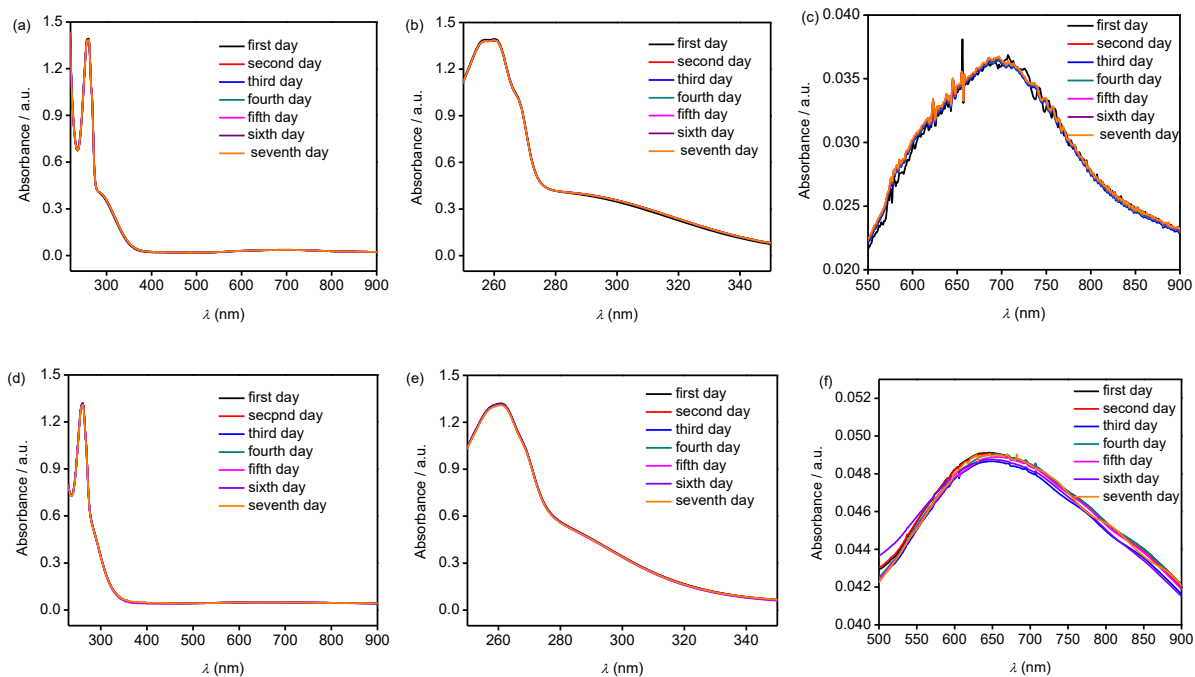


Fig. S7 Comparison of UV-vis spectra of pH 11.5 PBSs of (a), (b), (c) **1** and (d), (e), (f) **2** (**1** and **2** both in 0.1 mM) measured when freshly prepared and after stood for a week without protection of N_2 .

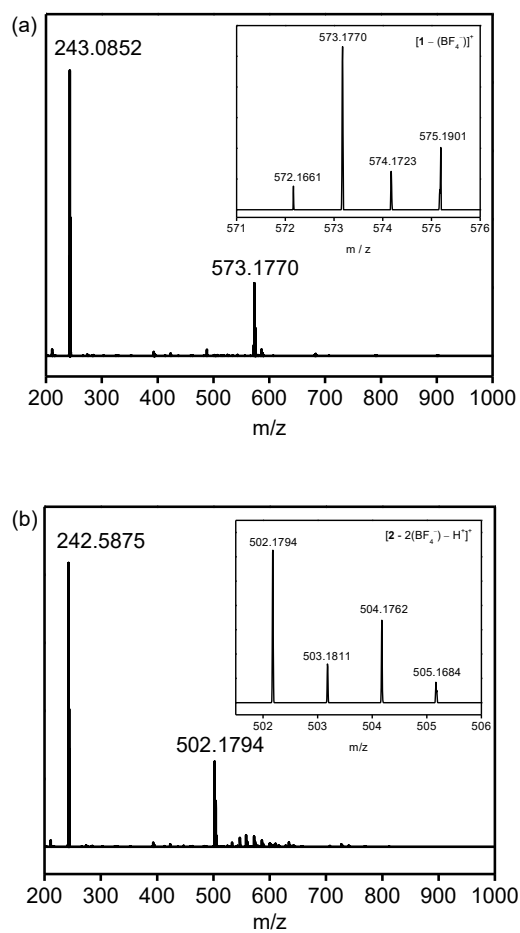


Fig. S8 High-resolution mass spectra (ESI, 3.5 kV) of (a) **1** and (b) **2** in 0.1 M PBSs at pH 11.5 after stood for a week without protection of N_2 . Insets: high-resolution mass spectra of $[1-(BF_4)]^+$ and $[2-2(BF_4)-H]^+$ peaks.

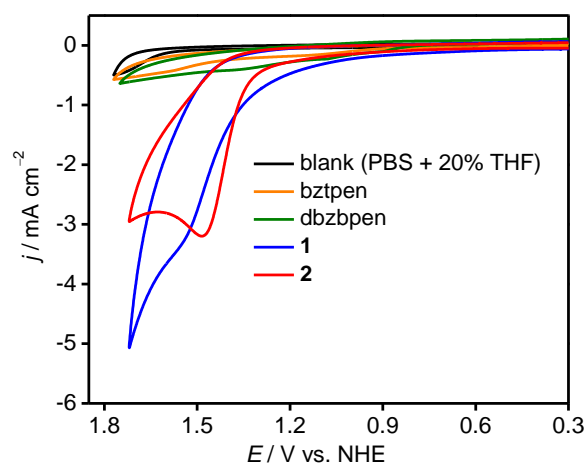


Fig. S9 Cyclic voltammograms of **1**, **2**, free bztpen and dbzbpn (all in 1.0 mM), and the blank cyclic voltammogram of a GC electrode. Complexes **1** and **2** in 0.1 M PBSs, ligands bztpen and dbzbpn in 0.1 M PBSs containing 20% THF (Ligands bztpen and dbzbpn could not be well dissolved in phosphate buffer), at pH 11.5 at a scan rate of 100 mV s^{-1} .

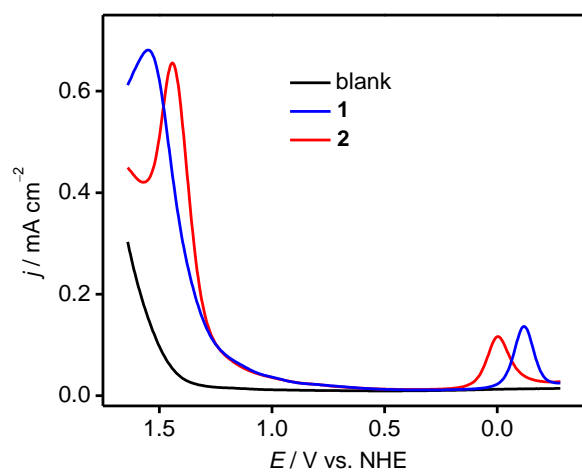


Fig. S10 Differential pulse voltammograms in the presence of 1.0 mM **1** or **2** in 0.1 M PBS at pH 11.5, and in the absence of catalyst, at a scan rate of 50 mV s^{-1} .

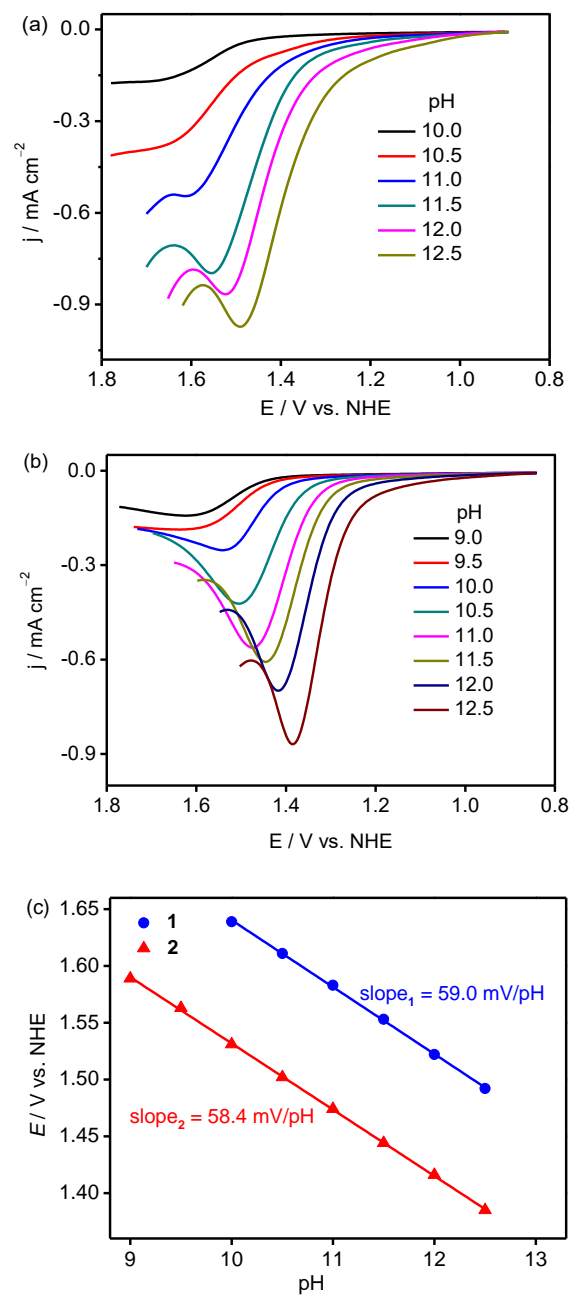


Fig. S11 Differential pulse voltammograms of (a) **1** (1.0 mM) in 0.1 M PBSs with pH varying from 10 to 12.5 and (b) **2** (1.0 mM) in 0.1 M PBSs with pH varying from 9.0 to 12.5. (c) Pourbaix diagram for **1** and **2**.

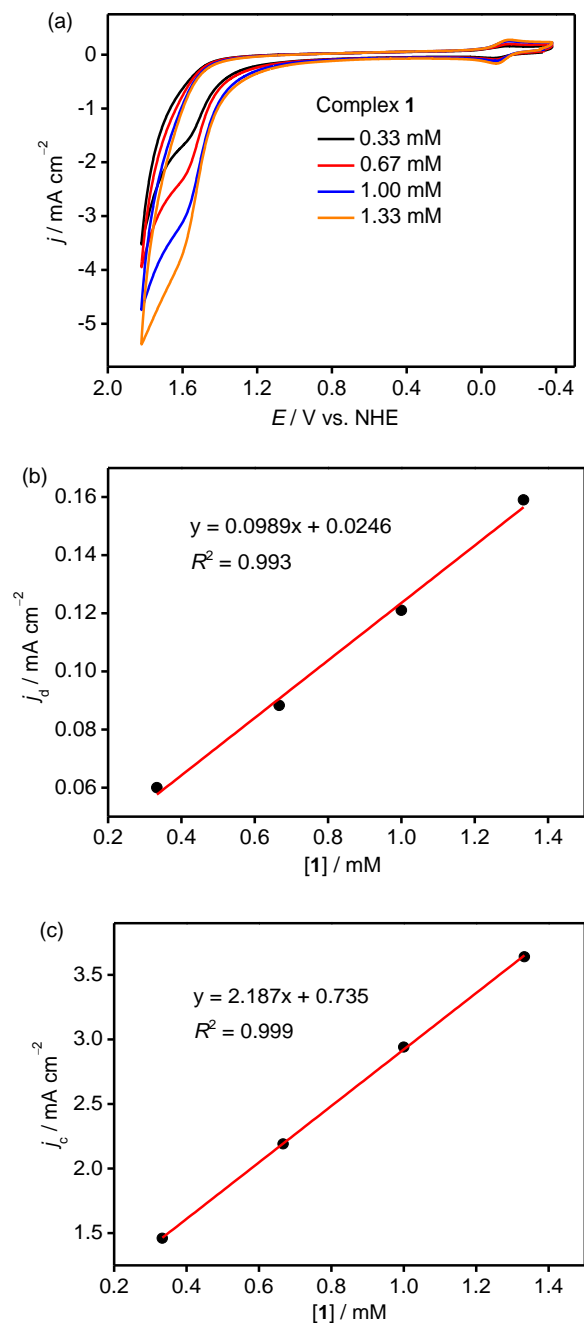


Fig. S12 (a) Cyclic voltammograms of **1** in 0.1 M PBSs at pH 11.5 at a scan rate of 100 mV s⁻¹ with the concentration of **1** varying from 0.33 to 1.33 mM. Plots of the current density maxima, j_d (b) and j_c (c), as a function of catalyst concentration.

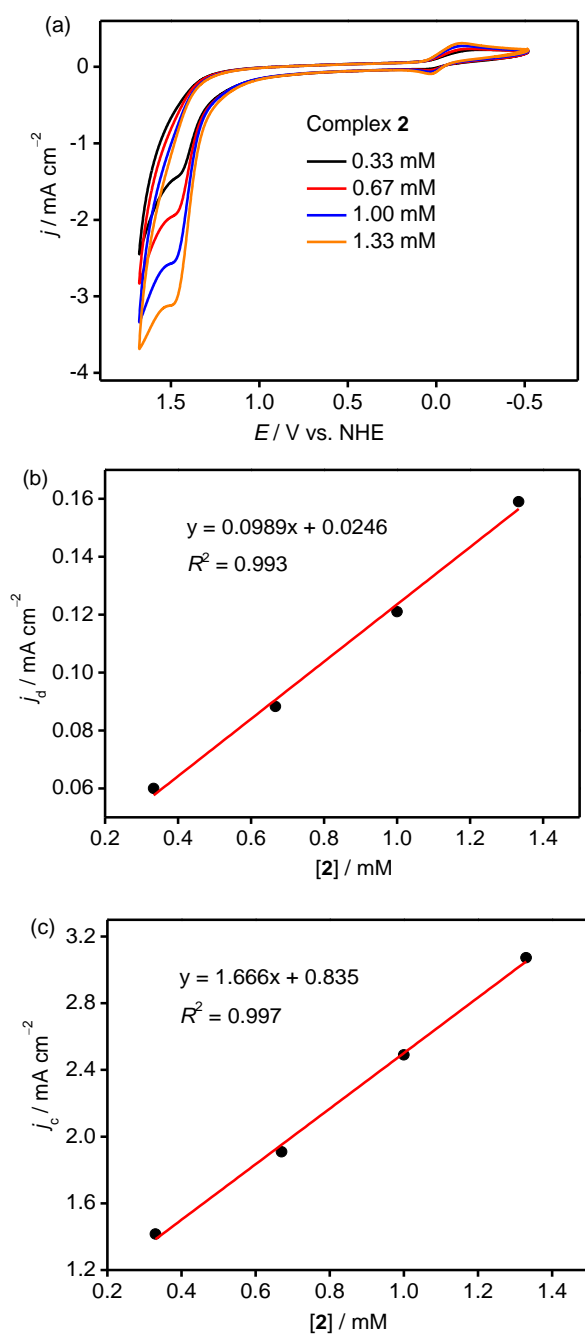


Fig. S13 (a) Cyclic voltammograms of **2** in 0.1 M PBSs at pH 11.5 at a scan rate of 100 mV s⁻¹ with the concentration of **2** varying from 0.33 to 1.33 mM. Plots of the current density maxima, j_d (b) and j_c (c), as a function of catalyst concentration.

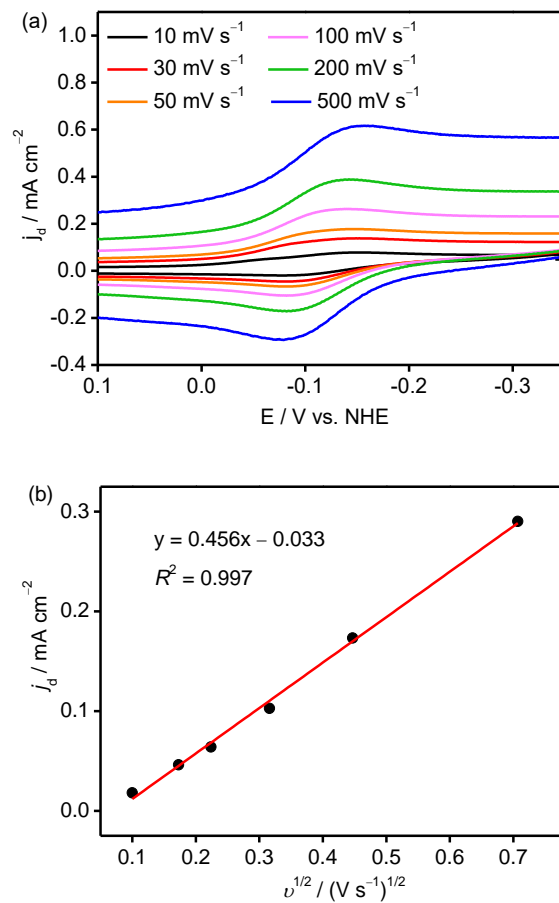


Fig. S14 (a) Cyclic voltammograms of **1** (1.0 mM) in 0.1 M PBSs at pH 11.5 with scan rate varying from 10 to 500 mV s^{-1} . (b) Plot of the anodic current density maximum of the $\text{Cu}^{\text{I}}/\text{Cu}^{\text{II}}$ couple as a function of the square root of scan rate.

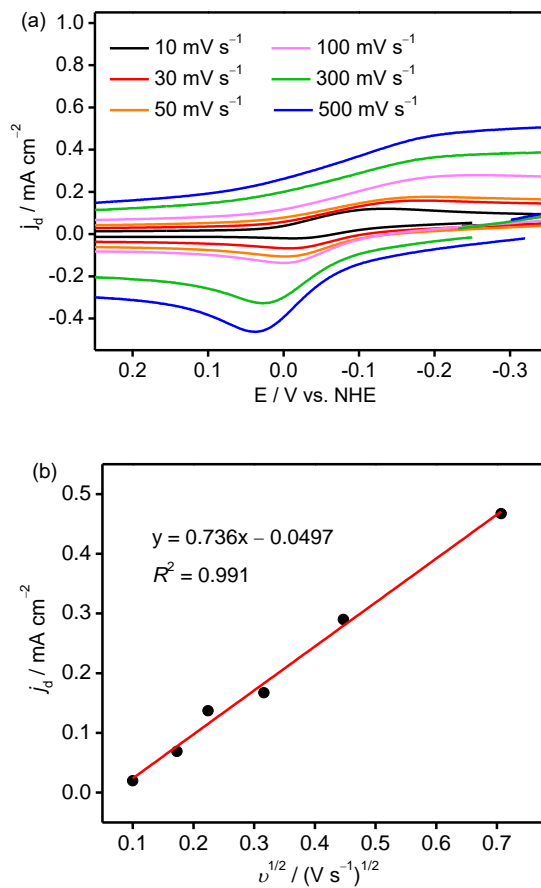


Fig. S15 (a) Cyclic voltammograms of **2** (1.0 mM) in 0.1 M PBSs at pH 11.5 with scan rate varying from 10 to 500 mV s^{-1} . (b) Plot of the anodic current density maximum of the $\text{Cu}^{\text{I}}/\text{Cu}^{\text{II}}$ couple as a function of the square root of scan rate.

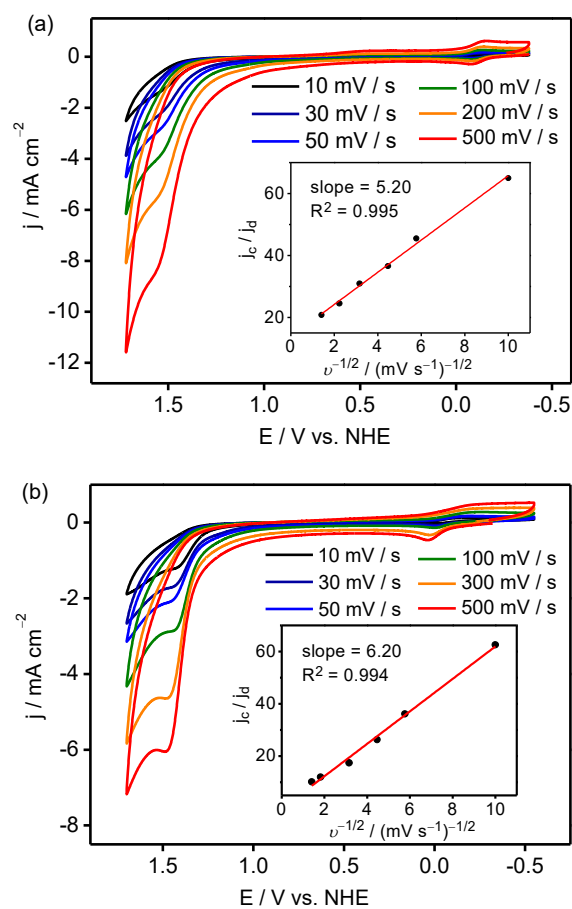


Fig. S16 Cyclic voltammograms of (a) **1** and (b) **2** (both in 1.0 mM) in 0.1 M PBSs at pH 11.5 at different scan rates (10–500 mV s⁻¹). Insets: plots of the ratio of j_c to j_a versus the reciprocal of the square root of scan rate.

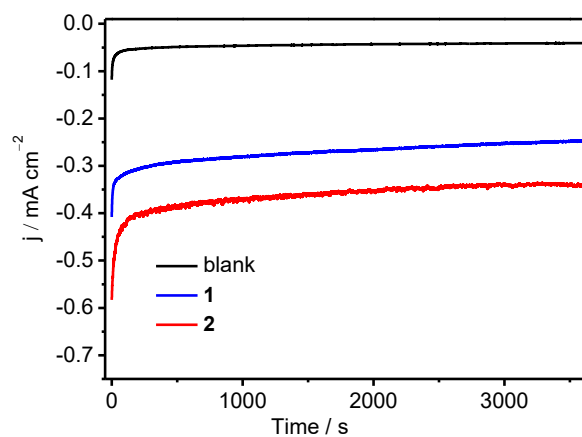


Fig. S17 Catalytic current obtained over 1 h in controlled potential electrolysis experiments without (blank) and with **1** and **2** (both in 1.0 mM) on a FTO electrode (0.70 cm²) at 1.40 V vs NHE in 0.1 M PBSs at pH 11.5.

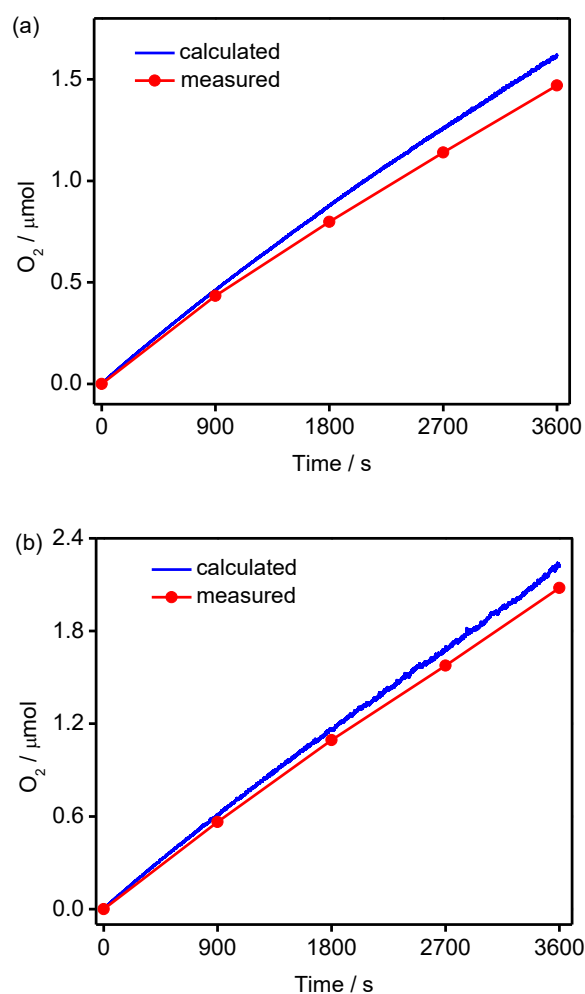


Fig. S18 Faradaic efficiencies of O₂ evolution for (a) **1** and (b) **2** in 0.1 M PBS at pH 11.5 at 1.4 V vs. NHE for 1 h of electrolysis. The red lines represent the amount of evolved O₂ quantified by GC analysis of the gas phase of the system, and the blue lines show the amount of O₂ expected for a 100% Faraday efficiency according to the passed charge during CPE experiment.

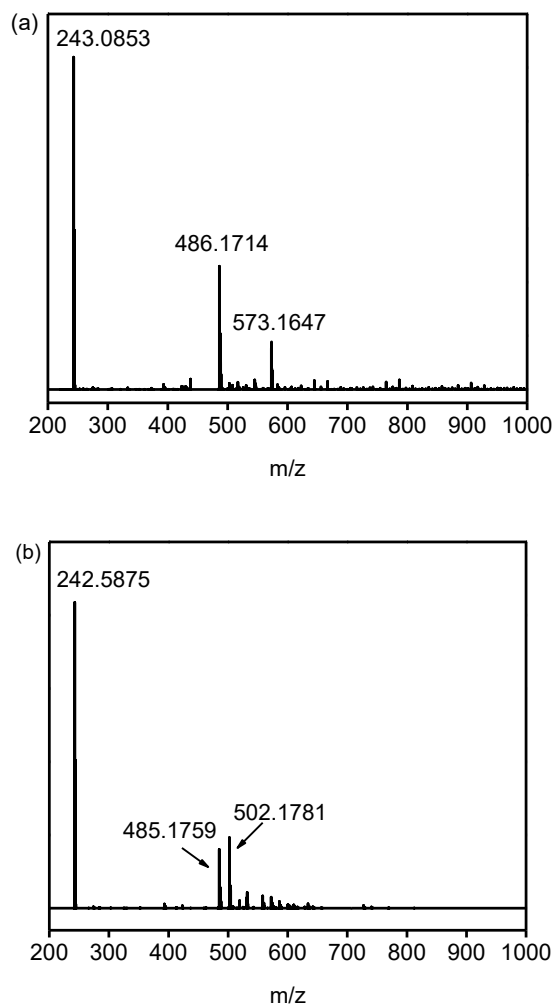


Fig. S19 High-resolution mass spectra (ESI, 3.5 kV) of the resulting electrolytes of (a) **1** and (b) **2** after 5 h of electrolysis. In Fig. S19a, $m/z = 243.0853$ for $[(\text{bztpen})\text{Cu}]^{2+}$, 573.1647 for $[(\text{bztpen})\text{Cu}(\text{BF}_4)]^+$, and 486.1714 for $[(\text{bztpen})\text{Cu}]^+$; in Fig. S19b, $m/z = 242.5875$ for $[(\text{dbzbpn})\text{Cu}]^{2+}$, 502.1781 for $[(\text{dbzbpn})\text{Cu}(\text{OH})]^+$, and 485.1759 for $[(\text{dbzbpn})\text{Cu}]^+$.

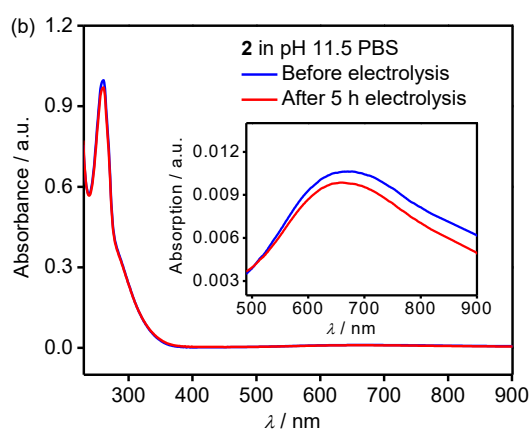
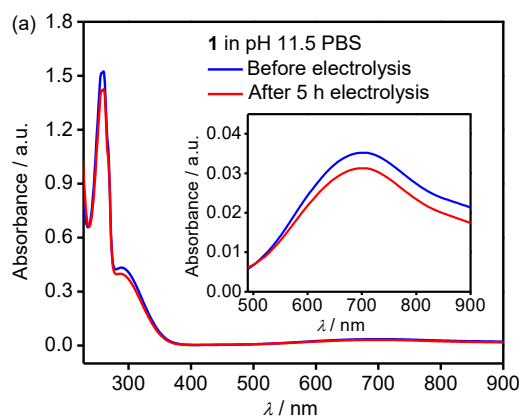


Fig. S20 UV-vis spectra of (a) **1** and (b) **2** in 0.1 M PBSs at pH 11.5 before and after electrolysis for 5 h. Insets: magnified views of the region of 500–900 nm.

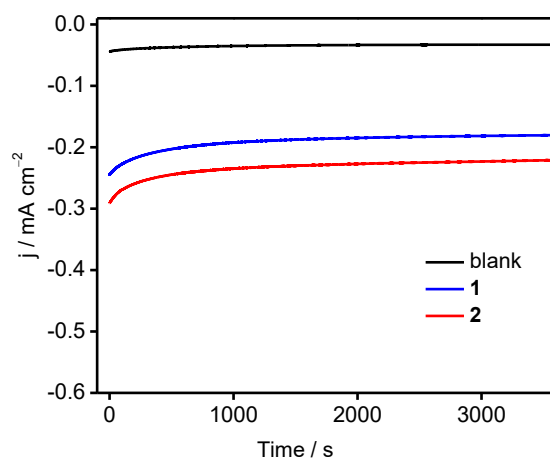


Fig. S21 Catalytic currents obtained over 1 h of CPE experiments without (blank) and with **1** or **2** (both in 1.0 mM) in 0.1 M PBS at pH 11.5 on a FTO electrode (0.70 cm²) at 1.40 V vs. NHE in an electrochemical cell with cathode and anode separated by a porous ceramic frit.

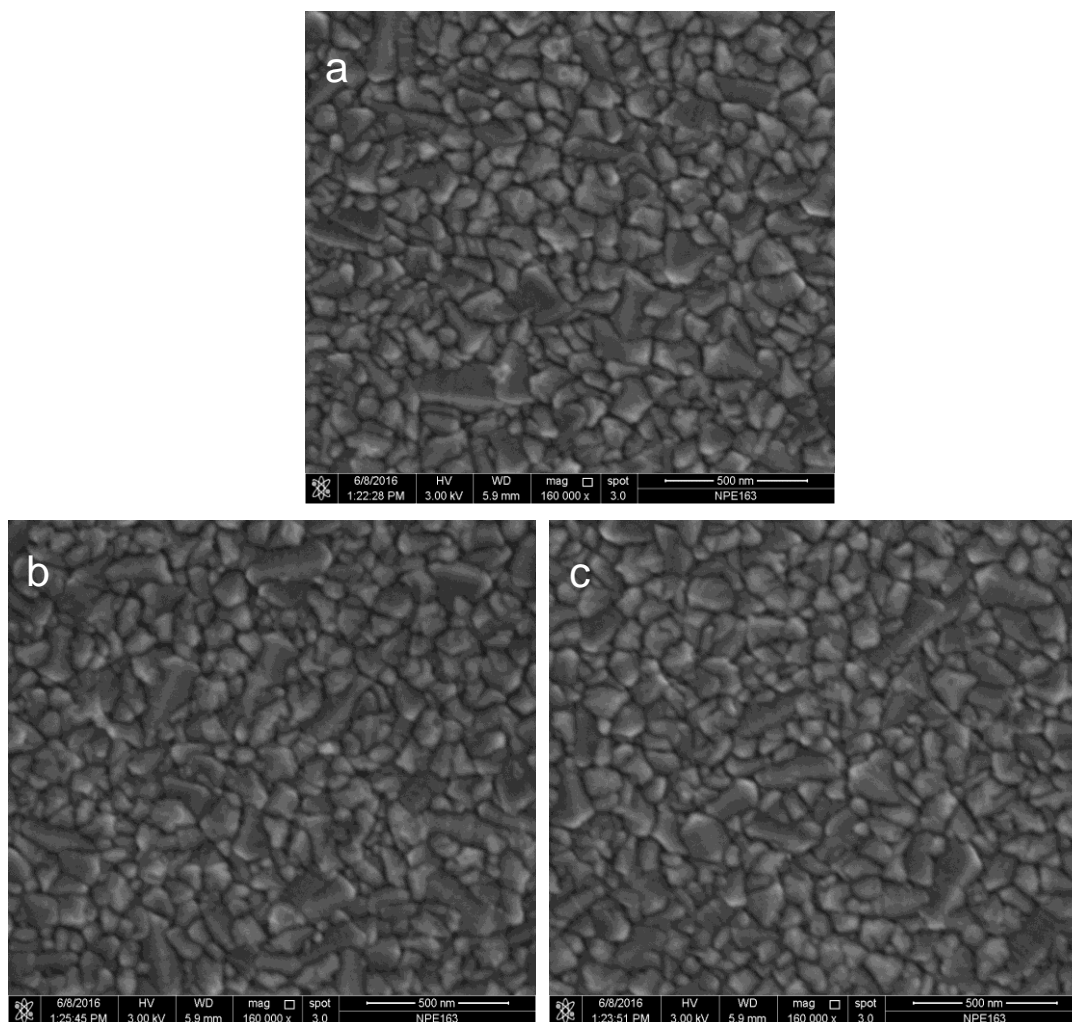


Fig. S22 SEM images of (a) a bare FTO before electrolysis, the FTO electrode after electrolysis for 5 h with (b) **1** or (c) **2** as an electrocatalyst.

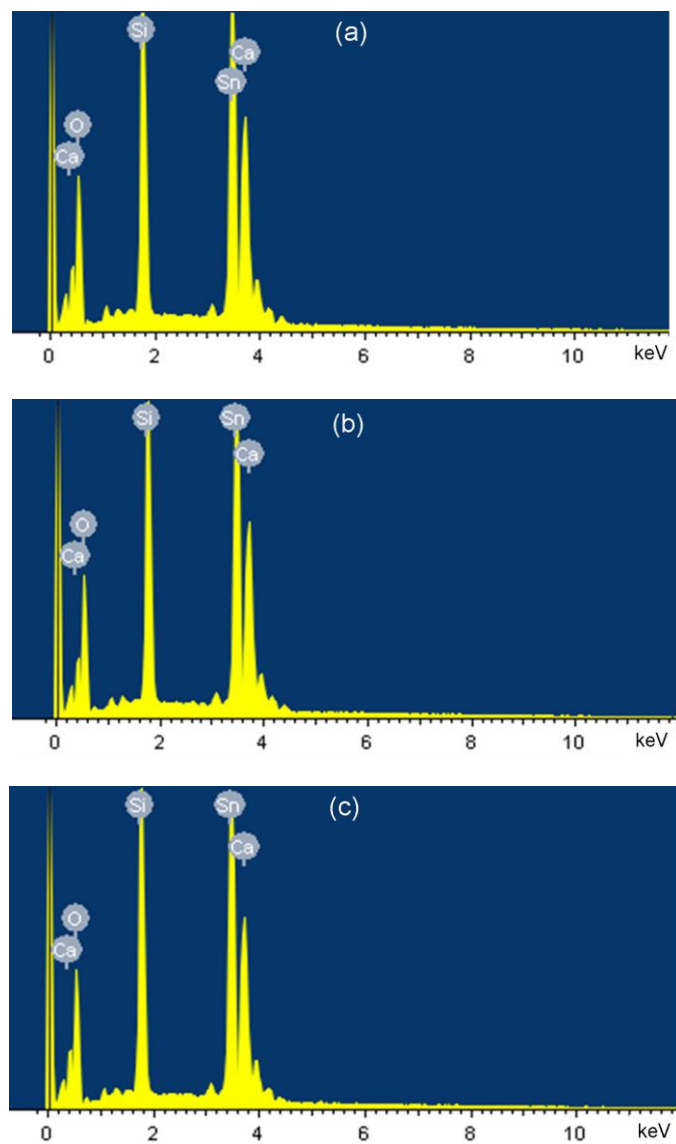


Fig. S23 EDX spectra of (a) a bare FTO before electrolysis, (b) after electrolysis for 5 h with **1** or (c) **2** as an electrocatalyst.

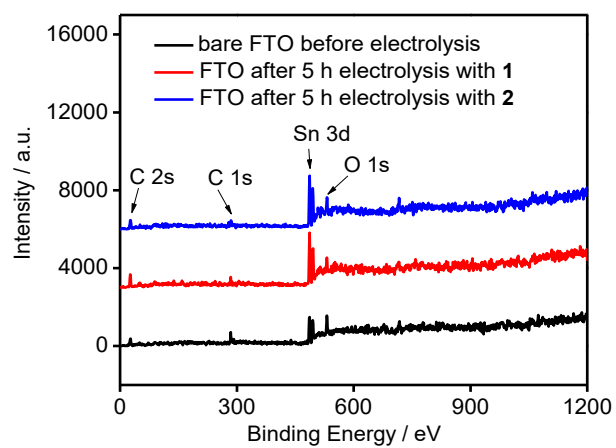


Fig. S24 XPS surveys of the FTO electrodes before and after electrolysis of **1** or **2** in 0.1 M PBS at pH 11.5 at 1.4 V for 5 h.

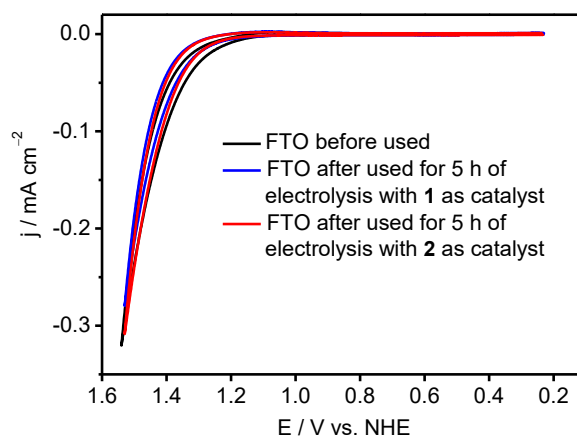


Fig. S25 Cyclic voltammograms of a 0.7 cm^2 FTO electrode and the FTO electrodes after 5 h of electrolysis with **1** and **2** as catalysts in 0.1 M PBSs at pH 11.5 at a scan rate of 100 mV s^{-1} .

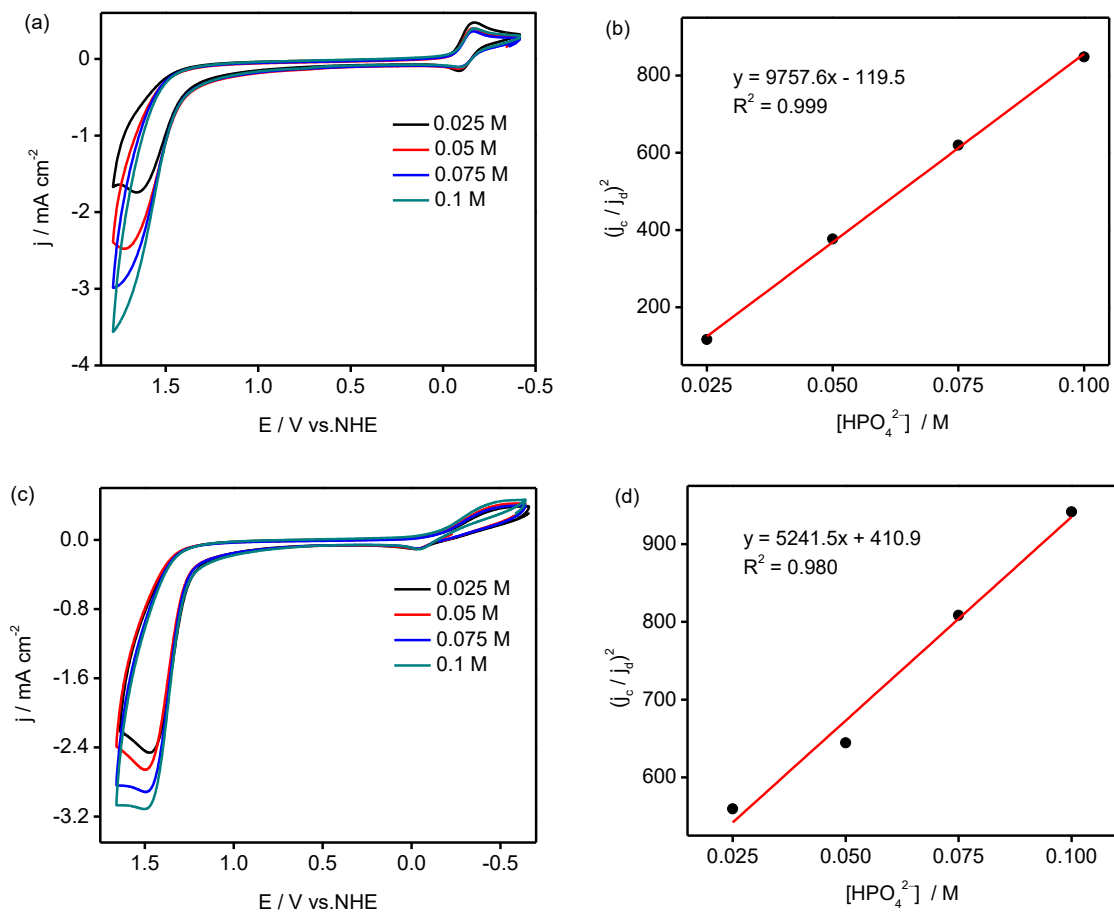


Fig. S26 Cyclic voltammograms of (a) **1** and (c) **2** (1.0 mM) at a scan rate of 100 mV s^{-1} with the concentration of phosphate buffer solution varied from 0.025 to 0.1 M at $\text{pH } 11.5$. Plots of $(j_c/j_d)^2$ as a function of $[\text{HPO}_4^{2-}]$ at constant concentration of (b) **1** and (d) **2**.

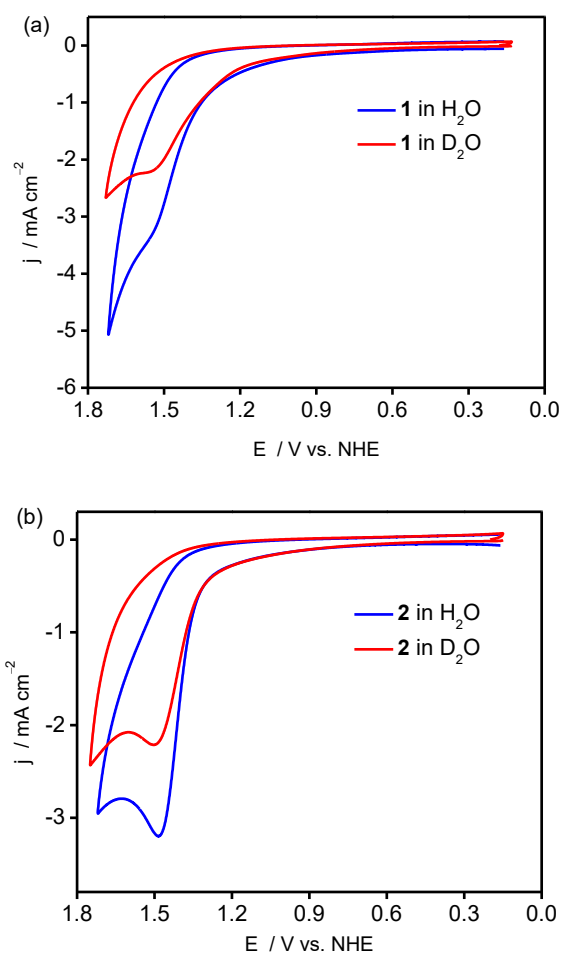


Fig. S27 Cyclic voltammograms of (a) **1** and (b) **2** in H₂O or D₂O phosphate buffer solution with glassy carbon as working electrode at a scan rate 100 mV s⁻¹. According to the equation of $k_{\text{cat,H}_2\text{O}}/k_{\text{cat,D}_2\text{O}} = (i_{\text{cat,H}_2\text{O}}/i_{\text{cat,D}_2\text{O}})^2$, KIE = 2.02 for **1** and 2.04 for **2**.

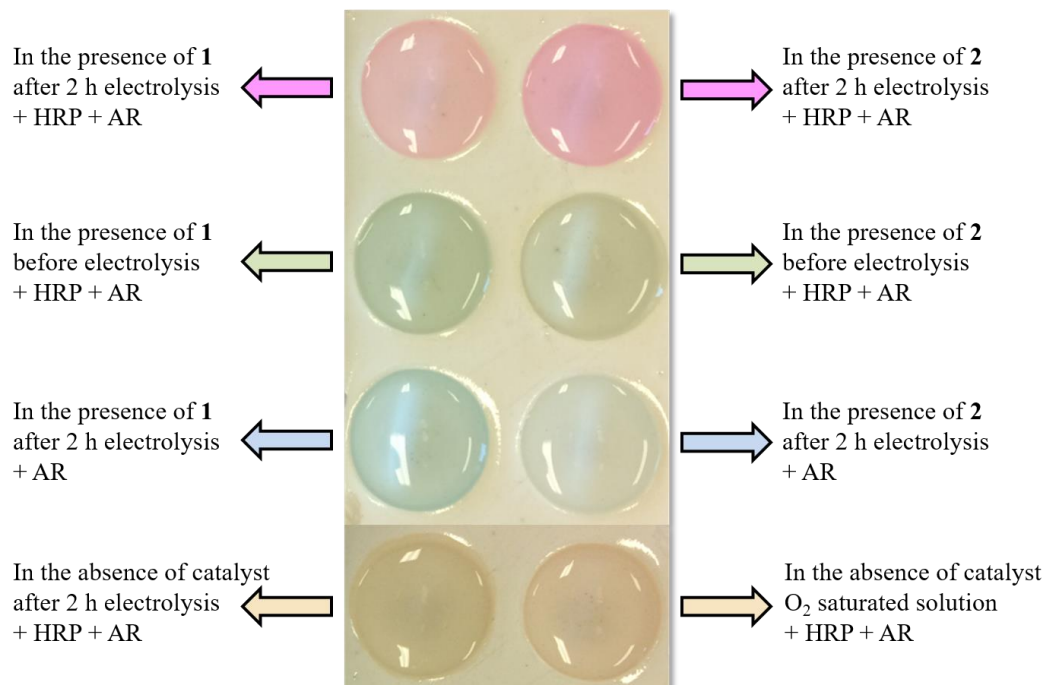


Fig. S28 Experiments for testing the peroxide intermediates in the resulting electrolytes after 2 h of electrolysis of **1** and **2** in pH 11.5 PBSs, using horseradish peroxidase (HRP, a special catalyst for hemolysis of the peroxide bond of H₂O₂ to form $\cdot\text{OH}$ radicals) and Ampliflu red (AR, a reliable titrant for $\cdot\text{OH}$).

Table S1 Crystallographic data and processing parameters for **1** and **2**

Complex	1 H ₂ O	2 CH ₃ OH
Formula	C ₂₇ H ₂₉ N ₅ B ₂ F ₈ Cu H ₂ O	C ₂₈ H ₃₂ N ₄ O ₂ B ₂ F ₈ Cu CH ₃ OH
Formula weight	660.71 + 18.01	677.75 + 32.03
Crystal system	Monoclinic	Orthorhombic
Space group	Cc	P2(1)2(1)2(1)
Z	4	4
<i>a</i> / Å	11.294(6)	11.5834(15)
<i>b</i> / Å	19.907(11)	13.5075(18)
<i>c</i> / Å	13.845(7)	20.031(3)
<i>α</i> / deg	90.00	90
<i>β</i> / deg	102.154(8)	90
<i>γ</i> / deg	90.00	90
<i>V</i> / Å ³	3043(3)	3134.0(7)
<i>D</i> _{calcd} / g m ⁻³	1.477	1.504
<i>μ</i> / mm ⁻¹	0.797	0.779
Crystal size / mm	0.20 × 0.16 × 0.13	0.17 × 0.14 × 0.13
<i>θ</i> Range / deg	2.05 / 28.19	2.32 / 27.43
Reflns collected / Indep.	4380 / 3642	7103 / 6521
Parameters refined	397	435
<i>F</i> (000)	1380	1460
GOF on <i>F</i> ²	1.045	1.047
Final <i>R</i> ₁ (<i>I</i> > 2(<i>I</i>))	0.0515	0.0605
Final <i>wR</i> ₂ (<i>I</i> > 2(<i>I</i>))	0.1586	0.1665
max. peak/hole / e Å ⁻³	0.530, -0.292	1.004 / -0.544

$$R_1 = \frac{\sum(|F_o| - |F_c|)}{\sum|F_o|}, wR_2 = \left[\frac{\sum(|F_o|^2 - |F_c|^2)^2}{\sum(F_o^2)} \right]^{1/2}$$

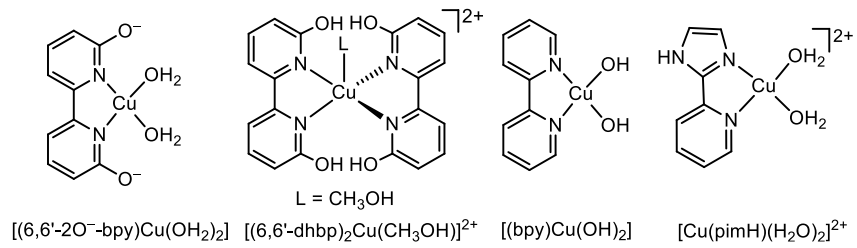
Table S2 Selected bond lengths (Å) and angles (deg) for **1** and **2**

Complex 1		Complex 2	
Bond lengths (Å)		Bond lengths (Å)	
Cu–N1	2.130(5)	Cu–N1	2.028(4)
Cu–N2	2.014(5)	Cu–N2	2.034(3)
Cu–N3	2.033(5)	Cu–N3	2.061(3)
Cu–N4	2.080(5)	Cu–N4	2.017(3)
Cu–N5	1.988(5)	Cu–O	2.194(3)
Bond angles (deg)		Bond angles (deg)	
N1–Cu–N2	108.8(2)	N1–Cu–N2	147.88(14)
N1–Cu–N3	81.7(2)	N1–Cu–N3	82.95(14)
N1–Cu–N4	106.07(17)	N1–Cu–N4	105.95(15)
N1–Cu–N5	107.81(19)	N1–Cu–O	91.53(14)
N2–Cu–N3	82.7(3)	N2–Cu–N3	85.89(13)
N2–Cu–N4	141.8(2)	N2–Cu–N4	82.14(14)
N2–Cu–N5	101.7(2)	N2–Cu–O	119.67(14)
N3–Cu–N4	87.4(2)	N3–Cu–N4	167.73(14)
N3–Cu–N5	167.2(2)	N3–Cu–O	96.51(14)
N4–Cu–N5	81.8(2)	N4–Cu–O	91.76(14)

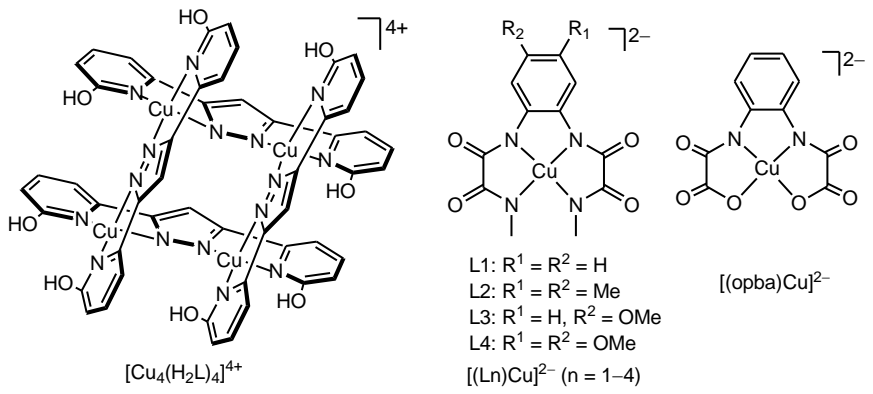
Table S3 Overpotentials and observed rate constants for copper complexes reported as WOCs

Entry	Catalyst ^a	pH	$\eta_{(\text{onset})}$ (mV)	k_{cat} (s ⁻¹)	Ref.
1	$[(6,6'-2\text{O}^- \text{-bpy})\text{Cu}(\text{H}_2\text{O})_2]$	12–14	510–560 (half peak potential)	0.4 (pH 12.4)	[S11]
2	$[(6,6'\text{-dhbp})_2\text{Cu}(\text{CH}_3\text{OH})]^{2+}$	12.6	477	0.356	[S12]
3	$[(\text{bpy})\text{Cu}(\text{OH})_2]$	12.5	510	100	[S13]
4	$[\text{Cu}_4(\text{H}_2\text{L})_4]^{4+}$	12.5	500	-	[S14]
5	$[\text{Cu}(\text{pimH})(\text{H}_2\text{O})_2]^{2+}$	12	330	35	[S15]
6	$[(\text{L1})\text{Cu}]^{2-}$	11.5	700	3.56	[S16]
7	$[(\text{L2})\text{Cu}]^{2-}$	11.5	400	3.58	[S16]
8	$[(\text{L3})\text{Cu}]^{2-}$	11.5	270	0.43	[S16]
9	$[(\text{L4})\text{Cu}]^{2-}$	11.5	170	0.16	[S16]
10	$[(2\text{GH}^{2-})\text{Cu}(\text{H}_2\text{O})]$	11	620	53	[S17]
11	$[(3\text{G}^{2-})\text{Cu}(\text{H}_2\text{O})]$	11	620	24	[S17]
12	$[(\text{TGG}^{4-})\text{Cu}(\text{H}_2\text{O})]^{2-}$	11	520	33	[S18]
13	$[(\text{opba})\text{Cu}]^{2-}$	10.8	636	1.13	[S19]
14	$[\text{Cu}(\text{Me}_2\text{oxpn})\text{Cu}(\text{OH})_2]$	10.4	636	2.14	[S20]
15	$[\text{Cu}(\text{oxpn})\text{Cu}(\text{OH})_2]$	10.1	289	6.7	[S21]
16	CuPcTS	9.5	570	-	[S22]
17	$[\text{Cu}(\text{F}_3\text{TPA})(\text{ClO}_4)(\text{CH}_3\text{CN})]^+$	8.5	610	0.38	[S23]
18	$[(\text{Py}_3\text{P})\text{Cu}]$	8	~ 430	20	[S24]
19	$[\text{Cu}(\text{en})_2]^{2+}$	8	~ 440	0.4	[S25]
20	$[\text{Cu}(\text{TMC})(\text{H}_2\text{O})]^{2+}$	7	580	30	[S26]
21	$[\text{Cu}_2(\text{BPMAN})(\mu\text{-OH})]^{3+}$	7	780	0.6	[S27]
22	$[\text{Cu}_4(\text{bpy})_4(\mu_2\text{-OH})_2(\mu_3\text{-OH})_2(\text{H}_2\text{O})_2]^{2+}$	7	730	-	[S28]
23	CuMe ₄ cyclam	7	880	~7	[S29]
24	$[(\text{bztpen})\text{Cu}]^{2+}$ (1)	11.5	440	13.1	This work
25	$[(\text{dbzbpn})\text{Cu}(\text{OH}_2)]^{2+}$ (2)	11.5	570	18.7	This work

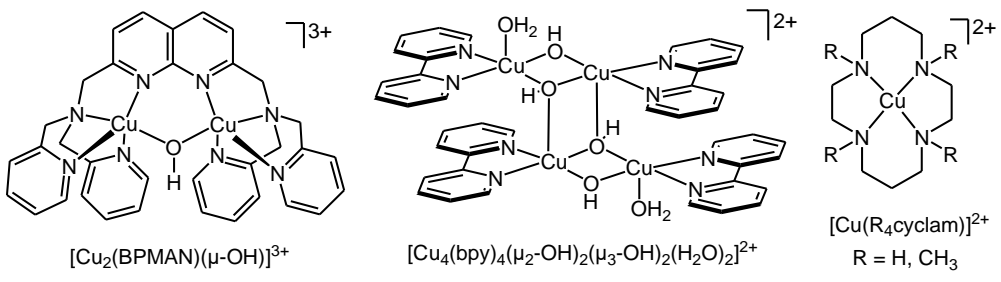
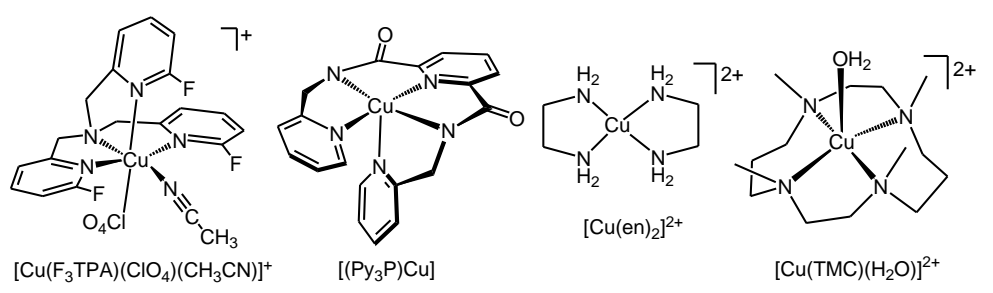
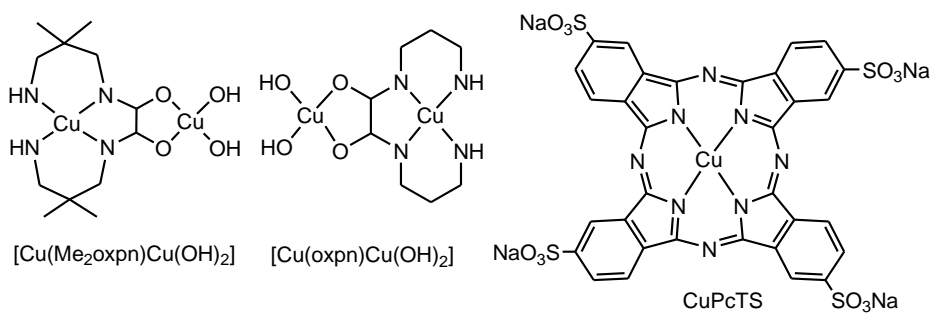
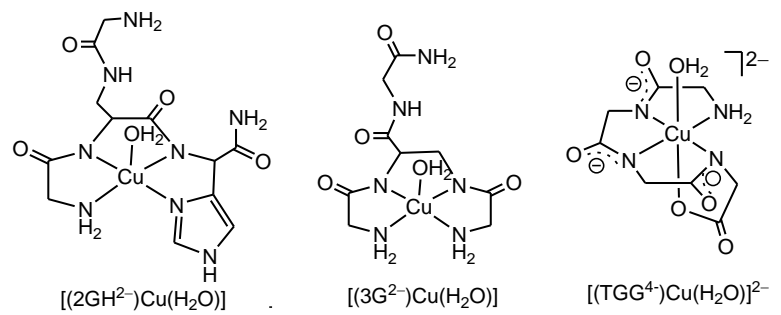
^aThe structures of the catalysts listed in Table S3 are given below.



L = CH₃OH



L1: R¹ = R² = H
 L2: R¹ = R² = Me
 L3: R¹ = H, R² = OMe
 L4: R¹ = R² = OMe



R = H, CH₃

Table S4 Estimation of decomposition extent of the copper catalyst during 5 h of electrolysis based on the UV-vis spectroscopic studies and the ICP analysis.

Complex	Attenuation of the UV-vis absorption ^a	Deposition of copper on the cathode from ICP analysis
1	ca. 67.36 μg (1.06 μmol) decomposed by 10.6%	ca. 59.10 \pm 2.54 μg (0.93 \pm 0.04 μmol) decomposed by 9.3%
2	ca. 45.12 μg (0.71 μmol) decomposed by 7.1%	ca. 37.49 \pm 3.45 μg (0.59 \pm 0.06 μmol) decomposed by 5.9%

^aThe estimation was based on the attenuation of the absorption at 700 nm for **1** and at 650 nm for **2**.

References

- [S1] M. V. de Almeida, A. P. S. Fontes, R. N. Berg, E. T. César, E. de C. A. Felício and J. D. de S. Filho, *Molecules*, 2002, **7**, 405–411.
- [S2] L. Duelund, R. Hazell, C. J. McKenzie, L. P. Nielsen and H. Toftlund, *J. Chem. Soc., Dalton Trans.*, 2001, 152–156.
- [S3] C. Ng, M. Sabat and C. L. Fraser, *Inorg. Chem.*, 1999, **38**, 5545–5556.
- [S4] P. Zhang, M. Wang, Y. Yang, T. Yao and L. Sun, *Angew. Chem. Int. Ed.*, 2014, **53**, 13803–13807.
- [S5] G. M. Sheldrick, SHELXTL97 Program for the Refinement of Crystal Structure, University of Göttingen, Germany, **1997**.
- [S6] Software packages SMART and SAINT, Siemens Energy & Automation Inc., Madison, Wisconsin, **1996**.
- [S7] G. M. Sheldrick, SADABS Absorption Correction Program, University of Göttingen, Germany, **1996**.
- [S8] A. J. Bard and L. R. Faulkner, *Electrochemical methods: Fundamentals and Applications*; Wiley: New York, 2001.
- [S9] V. Mishin, J. P. Gray, D. E. Heck, D. L. Laskin and J. D. Laskin, *Free Radical Biology & Medicine*, 2010, **48**, 1485–1491.
- [S10] U. S. Akhtar, E. L. Tae, Y. S. Chun, I. C. Hwang and K. B. Yoon, *ACS Catal.*, 2016, **6**, 8361–8369.
- [S11] T. Zhang, C. Wang, S. Liu, J.-L. Wang and W. Lin, *J. Am. Chem. Soc.*, 2014, **136**, 273–281.
- [S12] D. L. Gerlach, S. Bhagan, A. A. Cruce, D. B. Burks, I. Nieto, H. T. Truong, S. P. Kelley, C. J. Herbst-Gervasoni, K. L. Jernigan, M. K. Bowman, S. Pan, M. Zeller and E. T. Papish, *Inorg. Chem.*, 2014, **53**, 12689–12698.

- [S13] S. M. Barnett, K. I. Goldberg and J. M. Mayer, *Nat. Chem.*, 2012, **4**, 498–502.
- [S14] V. K. K. Praneeth, M. Kondo, P. M. Woi, M. Okamura and S. Masaoka, *ChemPlusChem.*, 2016, **81**, 1123–1128.
- [S15] L. A. Stott, K. E. Prosser, E. K. Berdichevsky, C. J. Walsby and J. J. Warren, *Chem. Commun.*, 2017, **53**, 651–654.
- [S16] P. Garrido-Barros, I. Funes-Ardoiz; S, Drouet, J. Benet-Buchholz, F. Maseras and A. Llobet, *J. Am. Chem. Soc.*, 2015, **137**, 6758–6761.
- [S17] J. S. Pap, L. Szyrwił, D. Sranko, Z. Kerner, B. Setner, Z. Szewczuk and W. Malinka, *Chem. Commun.*, 2015, **51**, 6322–6324.
- [S18] M.-T. Zhang, Z. Chen, P. Kang and T. J. Meyer, *J. Am. Chem. Soc.*, 2013, **135**, 2048–2051.
- [S19] L.-Z. Fu, T. Fang, L.-L. Zhou and S.-Z. Zhan, *RSC Adv.*, 2014, **4**, 53674–53680.
- [S20] L.-L. Zhou, T. Fang, J.-P. Cao, Z.-H. Zhu, X.-T. Su and S.-Z. Zhan, *J. Power Sources.*, 2015, **273**, 298–304.
- [S21] T. Fang, L.-Z. Fu, L.-L. Zhou and S.-Z. Zhan, *Electrochim. Acta.*, 2015, **161**, 388–394.
- [S22] R. Terao, T. Nakazono, A. R. Parent and K. Sakai, *ChemPlusChem.*, 2016, **81**, 1064–1067.
- [S23] R.-J. Xiang, H.-Y. Wang, Z.-J. Xin, C.-B. Li, Y.-X. Lu, X.-W. Gao, H.-M. Sun and R. Cao, *Chem. Eur. J.*, 2016, **22**, 1602–1067.
- [S24] M. K. Coggins, M. T. Zhang, N. Song and T. J. Meyer, *Angew. Chem. Int. Ed.*, 2014, **53**, 12226–12230.
- [S25] C. Lu, J. Du, X.-J. Su, M.-T. Zhang, X. Xu, T. J. Meyer and Z. Chen, *ACS Catal.*, 2016, **6**, 77–83.
- [S26] F. Yu, F. Li, J. Hu, L. Bai, Y. Zhu and L. Sun, *Chem. Commun.*, 2016, **52**, 10377–10380.

- [S27] X.-J. Su, M. Gao, L. Jiao, R.-Z. Liao, P. E. M. Siegbahn, J.-P. Cheng and M.-T. Zhang, *Angew. Chem. Int. Ed.*, 2015, **54**, 4909–4914.
- [S28] T.-T. Li and Y.-Q. Zheng, *Dalton Trans.*, 2016, **45**, 12685–12690.
- [S29] A. Prevedello, I. Bazzan, N. D. Carbonare, A. Giuliani, S. Bhardwaj, C. Africh, C. Cepek, R. Argazzi, M. Bonchio, S. Caramori, M. Robert and A. Sartorel, *Chem. Asian J.*, 2016, **11**, 1281–1287.